

Visualization of Rabi oscillations in a magnetic resonance

E. A. Ivanchenko*

*Institute for Theoretical Physics, National Science
Center “Institute of Physics and Technology”,
1, Akademicheskaya str., 61108 Kharkov, Ukraine*

(Dated: March 21, 2019)

Abstract

On the basis of solutions of the equations for a density matrix in Hermitian base the scheme of visualization of dynamics for the polarization vector of qudit in a time-dependent magnetic field is presented by means of mapping of the solution for the polarization vector on the three-dimensional spherical curve (vector hodograph). The received results obviously display the interference of precessional and nutational effects on the polarization vector in a magnetic resonance. The study can find practical applications in magnetic resonance and the 3D visualization of computational data.

PACS numbers: 87.63.L, 42.66.Si, 82.56.-b, 03.67.-a

Keywords: 3D Visualization, NMR, Quantum information

* eaiivanchenko1@gmail.com,yevgeny@kipt.kharkov.ua

I. INTRODUCTION

Imaging and visualization are among the most dynamic and innovative research areas of the past decades. This activity arises from the requirements of important practical applications such as the computational data visualization, the medical images processing for assisting medical diagnosis and intervention, and the 3D geometry reconstruction and processing for computer simulations. Due to the development of more powerful hardware resources, mathematical and physical methods, investigators have been incorporating advanced computational techniques to derive methodologies that can better enable the solution of the problems encountered.

In this paper we are going to introduce the 3D visualization scheme of the qudit polarization vector evolution in a magnetic field. As it is known, the magnetic resonance realization depends on the kind of the magnetic field modulations. Let's consider the spin dynamics in an alternating field [1, 2]

$$\overrightarrow{h}(t) = (h_1 \text{cn}(\omega t|k), h_2 \text{sn}(\omega t|k), H \text{dn}(\omega t|k)), \quad (1)$$

where cn , sn , dn are the Jacobi elliptic functions [3], ω is the field frequency. Such field modulation under the changing of the elliptic modulus k from 0 to 1 describes the whole class of field forms from trigonometric [4] ($\text{cn}(\omega t|0) = \cos \omega t$, $\text{sn}(\omega t|0) = \sin \omega t$, $\text{dn}(\omega t|0) = 1$) to the exponentially impulse ones ($\text{cn}(\omega t|1) = \frac{1}{\text{ch} \omega t}$, $\text{sn}(\omega t|1) = \text{th} \omega t$, $\text{dn}(\omega t|1) = \frac{1}{\text{ch} \omega t}$) [5]. The elliptic functions $\text{cn}(\omega t|k)$ and $\text{sn}(\omega t|k)$ have the real period $\frac{4K}{\omega}$, while the function $\text{dn}(\omega t|k)$ has a period of half the duration. Here K is the full elliptic integral of the first kind [3]. We call such field consistent.

At $k = 0$ and $h_1 = h_2 = h$ it is a circularly polarized magnetic field [4], where the scalar of the vector of the magnetic field does not depend on the time (a rotating magnetic field), and at $k = 0$ and $h_1 = h, h_2 = 0$ it is a linearly polarized field [6].

The solution of the Schrodinger equation for a wave function does not yield directly to the physical observed values. In the paper [7] real functions have been constructed from the Schrodinger equation solutions, which have direct physical sense and whose temporary evolution supposes visualization. The objective of this work is to present the visualization scheme of qudit polarization vector dynamics in a magnetic field on the base of both analytical and numerical solutions for the density matrix in the Hermitian base. The solution

represents a real generalized Bloch vector. The 3D sphere is used for the numerical simulation results visualization. The solution of the equations of motion for the polarization vector maps on tri-dimensional oriented spherical curve, which in the case of qudits shows a precession similar to that of a symmetric top in the gravitation field [8].

This paper is organized as follows. Section 2 describes in the presentation of the real Bloch vector a set of equations for qubit dynamics taking into account its environment. In Section 3 we present the 3D visualization scheme of the qudit polarization vector. On the base of the analytic solution in a rotating magnetic field the scheme of the qubit polarization vector visualization and the analytical formulas characterizing visualization in a resonance case, are presented in Section 4. Section 5 contains the analytical solution for qutrit in a rotating magnetic field in case of resonance, taking into account the anisotropy, as an example of the qudit polarization vector visualization. In Section 6 the results are presented pictorially at concrete parameters. The deductions are presented in the short conclusion. In the Appendix the subsidiary analytical results are added.

II. HAMILTONIAN AND MASTER EQUATION IN LINDBLAD FORM

The Hamiltonian of a magnetic qubit (spin 1/2 particle) which is in the external variable magnetic field $\vec{h}(t) = (h_1(t), h_2(t), h_3(t))$ is equal to

$$\hat{H} = h_i(t)s_i, \quad (2)$$

where $h_i(t)$ are the Cartesian components of the external magnetic field in frequency units (we suppose $\hbar = 1$); $s_i = \frac{1}{2}\sigma_i$, σ_i are the Pauli matrices.

The Liouville - Neumann equation for the density matrix ρ , describing the qubit dynamics and taking into account the environment in the form of Lindblad, takes the form

$$\partial_t \rho = -i[\hat{H}, \rho] + \frac{1}{2} \sum_{\alpha, \beta=1}^3 a_{\alpha\beta} (2\sigma_\alpha \rho \sigma_\beta - \sigma_\beta \sigma_\alpha \rho - \rho \sigma_\beta \sigma_\alpha), \quad \rho(t=0) = \rho_0, \quad (3)$$

where $a_{11} = a_{22} = \gamma_1/4$, $a_{33} = \gamma_2/2 - \gamma_1/4$, $a_{12} = a_{12}^* = -i\gamma_1 R_3(t=0)/4$, $a_{23} = a_{32} = a_{31} = a_{13} = 0$ [9, 10]. The constants γ_1 , γ_2 , and R_{eqr} are identified as the longitudinal and transverse lifetimes, and the equilibrium value of the population difference respectively.

We present the equation solution

$$\rho = \frac{1}{2} R_\alpha \sigma_\alpha, \quad \rho^+ = \rho, \quad \text{Tr } \rho = 1, \quad R_0 = 1, \quad (4)$$

in which, here and further, we imply the summation on repetitive Greek coefficients from zero to three and on Latin from one to three. The coherence vector (the Bloch vector) which is widely used in the theory of the magnetic resonance,

$$R_i = \text{Tr}(\rho\sigma_i), \quad (5)$$

characterizes the qubit behavior. At unitary evolution the length of the Bloch vector b is conserved

$$b = \sqrt{R_i^2}. \quad (6)$$

In the terms of functions R_i the Liouville - Neumann equation takes the form of the closed system of 3 differential equations for the Bloch vector components

$$\partial_t R_1 = h_2 R_3 - h_3 R_2 - \gamma_2 R_1, \quad (7)$$

$$\partial_t R_2 = h_3 R_1 - h_1 R_3 - \gamma_2 R_2, \quad (8)$$

$$\partial_t R_3 = h_1 R_2 - h_2 R_1 - \gamma_1 (R_3 - R_{egr}) \quad (9)$$

at the initially given conditions.

III. VISUALIZATION SCHEME OF DYNAMICS

One of the major stages of investigations is the visualization of the data obtained. "As known, the difficulty arising in quantum mechanics is not only to find the solutions but also to understand their meaning" [11]. In this paper it will be useful to map the solution for the polarization vector on geometrical model [7]. To this end, it is convenient to parameterize the unit polarization vector by spherical angles $(p_1, p_2, p_3) = (\sin \theta \cos \varphi, \sin \theta \sin \varphi, \cos \theta)$. Thus, the parameter φ ($0 \leq \varphi \leq 2\pi$) becomes a precession angle of the end of the vector \vec{p} on a sphere, referred to as apex, and the angle θ ($0 \leq \theta \leq \pi$) characterizes the nutation. $\theta = 0$ corresponds to the north pole on the sphere. These angles are expressed through the components of polarization vector \vec{p} according to the following formulae:

$$\theta(t) = \arccos p_3, \quad \sin \varphi(t) = \frac{p_2}{\sqrt{p_1^2 + p_2^2}}, \quad \cos \varphi(t) = \frac{p_1}{\sqrt{p_1^2 + p_2^2}}. \quad (10)$$

The angular velocities are given by

$$\theta'(t) = \frac{h_2 p_1 - h_1 p_2}{\sqrt{1 - p_3^2}}, \quad \varphi'(t) = \left(\arctan \frac{p_2}{p_1} \right)'. \quad (11)$$

The oriented spherical curve is characterized by the curvature k , torsion of the curve κ , velocity modulus of an apex v , and length of a path s . All these quantities can be easily calculated in terms of the components of polarization vector using the following formulae [12]:

$$k = \frac{|[\vec{p}', \vec{p}'']|}{|\vec{p}'|^3}, \kappa = \frac{(\vec{p}', \vec{p}'', \vec{p}''')}{[\vec{p}', \vec{p}'']^2}, v = \sqrt{p_1'^2 + p_2'^2 + p_3'^2}, s = \int_0^t v d\tau, \quad (12)$$

where the prime is used to denote the derivative with respect to time, $' \equiv \partial_t$. One can show [12] that the squared radius of adjoining sphere (in our case, a unit sphere) is related to a curvature, torsion, and velocity modulus of an apex by the formula

$$b^2 = 1 = \frac{1}{k^2} + \left(\frac{k'}{vk^2\kappa}\right)^2. \quad (13)$$

For the closed trajectories it is possible to introduce the integral characteristics:

$$C = \oint_{\Gamma} \vec{p}' \cdot d\vec{p}, L = \oint_{\Gamma_1} \oint_{\Gamma_2} \frac{d\vec{p}_1' \cdot d\vec{p}_2'}{|\vec{p}_1' - \vec{p}_2'|}, \quad (14)$$

where C is a circulation of vector \vec{p}' along the closed path Γ . For two spins L is a geometrical quantity (mutual induction ratio) in which the element of length $d\vec{p}_1' \in \Gamma_1$ is multiplied scalarwise on $d\vec{p}_2' \in \Gamma_2$ and product is divided into the distance of these elements from each other. This parameter depends only on a configuration and a relative position of contours, as well as on a choice of a direction of positive bypass of each contour.

IV. RABI MODULATION

Taking into account the environment with parameters $\gamma_2 = \gamma_1 = \gamma, R_{eqr} = 0$, in terms of the Bloch vector the Rabi model [4] is described by a matrix equation with an initial state $R(t=0) = (R_1(t=0), R_2(t=0), R_3(t=0))^T$ (here T indicates transposition)

$$\partial_t R = MR, \quad (15)$$

where the matrix looks as $M = \begin{pmatrix} \gamma & -H & h \sin \omega t \\ H & \gamma & -h \cos \omega t \\ -h \sin \omega t & h \cos \omega t & \gamma \end{pmatrix}$.

Let's introduce vector $r = aR$ in which the orthogonal matrix is equal to

$$a = \begin{pmatrix} \cos \omega t & \sin \omega t & 0 \\ -\sin \omega t & \cos \omega t & 0 \\ 0 & 0 & 1 \end{pmatrix}. \text{ The equation for } r \text{ takes the form}$$

$$\partial_t r = \tilde{M}r \quad (16)$$

with the constant matrix $\tilde{M} = \begin{pmatrix} \gamma & -\delta & 0 \\ \delta & \gamma & -h \\ 0 & h & \gamma \end{pmatrix}$. Now the solution can be written as: $R = a^{-1}e^{\tilde{M}t}R(t=0)$. For the initial state $R(t=0) = (\cos\varphi_0 \sin\theta_0, \sin\varphi_0 \sin\theta_0, \cos\theta_0)^T$ for $\varphi_0 = \theta_0 = 0$ the solution becomes

$$R_1 = \frac{he^{-\gamma t}}{\Omega^2}(\Omega \sin \Omega t \sin \omega t + \delta(1 - \cos \Omega t) \cos \omega t), \quad (17)$$

$$R_2 = \frac{he^{-\gamma t}}{\Omega^2}(\delta(1 - \cos \Omega t) \sin \omega t - \Omega \sin \Omega t \cos \omega t), \quad (18)$$

$$R_3 = \frac{e^{-\gamma t}}{\Omega^2}(\delta^2 + h^2 \cos \Omega t), \quad (19)$$

where $\delta = H - \omega$ and $\Omega = \sqrt{\delta^2 + h^2}$ is the nonresonance Rabi frequency.

The spin-flip probability is equal to

$$P = \frac{1 - R_3}{2}. \quad (20)$$

This probability at a resonance $\delta = H - \omega = 0$ has an oscillating behavior and also reaches a unity. At big detuning $\delta \gg 1$ the spin-flip probability tends to zero. If the longitudinal field $H = 0$, then the peak probability is equal to 1/2.

In the case of the elliptic field (1), as the expansion of the Rabi model, the solution in the elliptic field is the following:

$$R_1 = e^{-\gamma t} \text{sn}(\omega t|k) \sin ht, R_2 = -e^{-\gamma t} \text{cn}(\omega t|k) \sin ht, R_3 = e^{-\gamma t} \cos ht. \quad (21)$$

In the model under consideration, the Bloch vector components decay in due course, but the unit polarization vector $\vec{p} = (p_1, p_2, p_3)$ does not depend on γ .

A. Visualization of dynamics in a circularly polarized field

Let's give results for the explicit solution of the Rabi model for the initial state $\varphi_0 = \theta_0 = 0$. In the circularly polarized field $\vec{h}(t) = (h \cos \omega t, h \sin \omega t, H)$ the nutation and precession velocities have the form

$$\theta' = \frac{h^2 \Omega \sin \Omega t}{\sqrt{\Omega^4 - (\delta^2 + h^2 \cos \Omega t)^2}}, \quad \varphi' = \frac{\omega \delta^2 + \Omega^2 \delta + \omega \Omega^2 - \omega (\delta^2 - \Omega^2) \cos \Omega t}{\delta^2 + \Omega^2 + (\Omega^2 - \delta^2) \cos \Omega t}. \quad (22)$$

But in the case of resonance, the nutation velocity is the constant and the precession velocity is the constant too

$$\theta'(\delta = 0) = h \text{sgn}(\sin ht), \quad \varphi'(\delta = 0) = \omega \quad (23)$$

with the period $T = 2\pi/h$.

The curvature, torsion, velocity, path length and circulation at the exact resonance are expressed by the formulae

$$k_{res} = \frac{\sqrt{(h^2 + 3\omega^2)(8h^4 + 4\omega^2h^2 + \omega^4) - g(t)}}{(2h^2 + \omega^2 - \omega^2 \cos 2ht)^{3/2}}, \quad (24)$$

$$\kappa_{res} = -\frac{4h\omega(4h^4 + 7\omega^2h^2 + \omega^4 + \omega^2(h^2 - \omega^2)\cos 2ht)\sin ht}{(h^2 + 3\omega^2)(8h^4 + 4\omega^2h^2 + \omega^4) - g(t)}, \quad (25)$$

$$v_{res} = \frac{1}{\sqrt{2}}\sqrt{2h^2 + \omega^2 - \omega^2 \cos 2ht}, \quad (26)$$

$$s_{res} = F(ht | -\frac{\omega^2}{h^2}), \quad C_{res} = 2\pi h + \frac{\pi\omega^2}{h}, \quad (27)$$

where $g(t) = 4(\omega^4 - h^4 + 3\omega^2h^2)\omega^2 \cos 2ht + (\omega^2 - h^2)\omega^4 \cos 4ht$,

$F(\phi|m) = \int_0^\phi (1 - m \sin^2 \vartheta)^{1/2} d\vartheta$ is the elliptic integral of the second kind.

In the consistent Rabi field (cRf) Eq. (1), at the resonance, the angular velocities depend on the time and are equal to

$$\theta_{cRf}'(\delta = 0) = h \operatorname{sgn}(\sin ht), \quad \varphi_{cRf}'(\delta = 0) = \omega \operatorname{dn}(\omega t | k). \quad (28)$$

V. SPIN $S > 1/2$

The qudit is characterized by the generalized Bloch vector, the dimension of which is equal to $(2S + 1)^2 - 1$. The so developed scheme for a spin 1/2 is completely applicable for qudits, for the polarization vector visualization and the anisotropy influence on polarization. For the qutrit, the 2D parametric time dependence of the Bloch vector components, was studied [13, 14].

The Hamiltonian of the spin 1 (qutrit) in a external variable magnetic field $\vec{h}(t)$ taking into account anisotropy has the form [15]

$$\hat{H}(h, Q, d) = h_i(t)S_i + Q(S_3^2 - \frac{2}{3}E_{3 \times 3}) + d(S_1^2 - S_2^2), \quad (29)$$

where S_i are the spin matrixes and the anisotropy constants Q, d take account of the contributions of the one-quantum and double-quantum transitions in qutrit [15]. The explicit form of the spin matrices and the set of equations, determining the qutrit evolution are given in the paper [15]. The exact solution in the circularly polarized field at the resonance without the influence of constant d is given in the Appendix Eqs. (31)-(38).

For the closed paths at $\omega = 0$ in the solution (31)-(38) the requirement of the frequency commensurability at $d = 0$ looks as $m\sqrt{4h^2 + Q^2} = nQ$, from which it follows that

$$h = \pm\sqrt{n^2 - m^2}\frac{Q}{2m}, \quad (30)$$

where n, m are the integer numbers. It is possible to show that the condition for the closed trajectory at $d \neq 0$ has the form $h + \sqrt{2}d = \pm\sqrt{n^2 - m^2}\frac{Q}{2m}$.

VI. NUMERICAL RESULTS

Qubit. In the circularly polarized field in Fig. 1 the curvature, torsion and velocities are presented, which for descriptive reasons are combined by introducing a scale factor (for the curvature). It becomes clear that when the torsion κ changes its sign from plus to minus, the velocity modulus of the apex $v \equiv |\vec{p}'|$ decreases, the precession velocity is minimum, the nutation velocity changes its sign from minus to plus and the curvature k increases. The interaction of the effects of precession and nutation is geometrically described in Fig. 2. The occurrence of loops (self-superposition) follows from the fact that the precession velocity on the upper parallel is opposite to the velocity on the lower parallel.

At the cusps, as it is obvious in Fig. 3, there is a sharp transition from some geometrical characteristics of the hodograph to others (that is, linking trajectories with different k, κ). In the transition vicinity the velocity v sharply decreases [16], the curvature and torsion sharply increase and the precession and nutation velocities tend to zero.

If motion begins from $\theta = 0$ or $\theta = \pi$, then the upper or accordingly the lower parallel of the sphere degenerates in the point. Fig. 4 presents dynamics, where in the vicinity of the cusps the velocity v sharply decreases, the curvature and torsion sharply increase, and the precession and nutation velocities actually transit through zero. In all the cases in the cusps the qubit energy $E_{Rabi} = \text{Tr}(\rho\hat{H})$ has its local maximum.

At the coincidence of the external field frequency and the eigenfrequency there is the resonance in the system. On the sphere in Fig. 5 it is visible that at very small frequencies which correspond to the small precession velocity Eq. (23), on the closed apex trajectories (with beginning on the northern pole towards the southern one and termination on the northern pole for one period), which is a purely periodic driving with a period $T = 2\pi/h$, there are no self-intersections. At the constant Rabi frequency h , (see Fig. 6), the increase of

the frequency ω causes the increase of the path length. Let's emphasize that the trajectory is not flat, but tri-dimensional. This is visible along the path, which is more than 2π , and by means of another criteria it is possible to show that for the plane curve torsion is equal to zero in each point. The whole class of closed trajectories satisfies the requirement for the closed curve which is determined by the formula $h = \pm\sqrt{n^2\omega^2/m^2 - (H - \omega)^2}$.

As it is known [6], in the linearly polarized field $\vec{h}(t) = (h \cos \omega t, 0, H)$, the resonance happens at $\omega \neq H$, (the Bloch-Siegert resonance frequency shift). The visualization for such modulation was partially considered in the paper [16]. We would like only to add that in the linearly polarized field instead of loops or cusps, the hodograph obtained from the numerical solution, at parameters such as in Fig. 3 is more smooth (see Fig. 7) as the precession velocity does not change its sign and the curvature and torsion in such field are much less than in the rotating field.

Qutrit. We present some numerical results describing qutrit dynamics in the field $\vec{h}(t) = (h, 0, 0)$ for $d = 0$. The smooth closed trajectory goes through the both poles that means that there is a two-photon transition. In more detail, a flip of the third component of polarization vector π_3 occurs and the population of the lowest level P_{-1} is equal to unity over the time $(5(2\pi/f))$. In the vicinity of the southern pole, the precession velocity takes its minimum value and the nutation velocity changes its sign from plus to minus. Fig. 8 shows both dynamics of the level populations with spin projections (1,0,-1) and third projection of the polarization vector π_3 . Fig. 9 presents the dynamics of velocities. A comparison with the hodograph, given in Fig. 10, shows that the precession corresponds to small oscillations of π_3 (two orbits on the sphere over the time $2(2\pi/f)$). Then the sharp nutational change of π_3 (the smooth curve) occurs during $(2\pi/f)$. Next four precessional orbits go through the south pole of the sphere during $4(2\pi/f)$. Further sharp nutational change of π_3 (the smooth curve) takes place during $(2\pi/f)$. The full period $10(2\pi/f)$ is completed by two precessional orbits on the northern pole of the sphere over the time $2(2\pi/f)$. In other words, there is a quasitrapping π_3 on the poles. All the velocities v, φ', θ' grow with increasing anisotropy and the periods of "hodograph components" decrease. However, the shape of hodograph does not depend on the anisotropy parameter at positive Q . The torsion κ is small and repeatedly changes its sign during the full period. In fact, such a hodograph is the Lissajous figure on the tri-dimensional sphere.

The influence of the anisotropy constant d caused by the double-quantum transitions

leads to the increase of the transition frequency. When $d = 0.1$, the frequency of the double-quantum transitions is increased approximately twice, due to reduction of the number of the precessional orbits on the poles.

2 qutrits. Having solved equation system for two qutrits with the Hamiltonian $\hat{H}_2 = \hat{H}(h, Q, d) \otimes E_{3 \times 3} + E_{3 \times 3} \otimes \hat{H}(\bar{h}, \bar{Q}, \bar{d}) + J\vec{S} \otimes \vec{S}$ numerically [15] in the constant magnetic field with the isotropic interaction and the initial state of the antiparallel polarization vectors pointed at poles of the sphere (see Fig. 11), we find the mutual induction ratio dependence on an exchange constant: $L(J = -0.01) = -5.61$, $L(J = 0) = -5.81$, $L(J = 0.01) = -5.93$.

The results obtained well exhibit quantum interference of the precession and nutation components of the motion of the polarization vector in resonance and nonresonance conditions.

VII. CONCLUSION

A system of closed equations describing dynamics of the Bloch vector components for a qubit in an arbitrary time-dependent external magnetic field is derived. On the basis of analytical solutions we propose a scheme of the qubit dynamics visualization. This is realized by mapping the solution on a tri-dimensional parametric hodograph of an apex of polarization vector on a sphere. The numerical results for the qubit dynamics in a circularly polarized field are presented for different initial states. Such representation and its numerical validation are important also in view of a deeper insight in the relation between classical and quantum randomness, opening unexpected, possible applications of the mathematical formalism of quantum mechanics in other domains of science. The proposed scheme of visualization is also applicable for 3D mapping the analytical or numerical solution of coupled qudits.

We believe that this study will be useful since 3D visualization of polarization vectors can be applicable to a double magnetic resonance and manipulations of quantum bits. The visualization may have potential applications in magnetometry and quantum information processing.

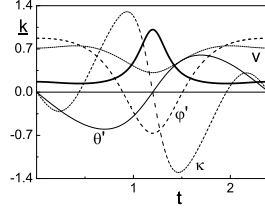


Fig. 1. Time dependencies of the curvature k , torsion κ , velocity v , precession and nutation velocities φ' , θ' , for the initial state $\theta_0 = \arccos \frac{1}{\sqrt{3}}$, $\varphi_0 = 0$ with the parameters of the circularly polarized field $\omega = 3$, $H = 0.45$, $h = -0.6$; $\underline{k} = k/20$ during $2\pi/\Omega$.

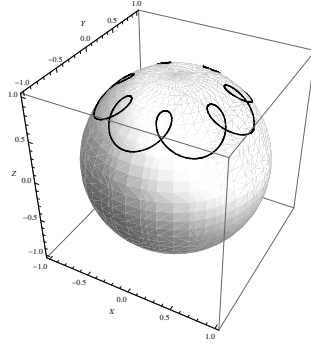


Fig. 2. Mapping of the qubit dynamics on the apex hodograph (quantum interference of precession and nutation) with the parameters as in Fig. 1 for total time $T_{all} = 7(2\pi/\Omega)$. The spin-flip probability oscillates in the limits of $0.06 \leq P \leq 0.211$. The path length equals $s = 10.44$.

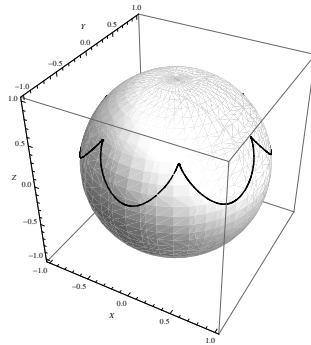


Fig. 3. Cusps at $\theta_0 = \arccos \frac{1}{\sqrt{3}}$, $\varphi_0 = \pi/4$; $\omega = 3$, $H = 0.5$, $h = 0.6$ during $6(2\pi/\Omega)$; $0.19 \leq P \leq 0.4$; $0.015 \leq v \leq 0.78$, $-0.02 \leq \varphi_t \leq 0.67$, $-0.6 \leq \theta_t \leq 0.6$, $1 \leq k \leq 8500$, $-1550 \leq \kappa \leq 1550$, $s = 8.6$.

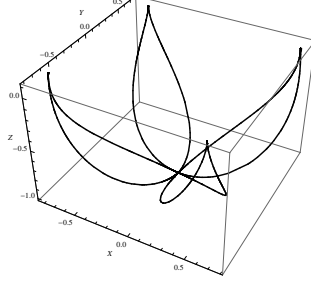


Fig. 4. 3D parametric plot of the qubit polarization vector $\vec{p}(t)$ vs. time. $\theta_0 = \pi$, $\varphi_0 = 3\pi/4$; $\omega = 0.5$, $H = 0.05$, $h = 0.5$ during $4(2\pi/\Omega)$; $0.005 \leq v \leq 0.5$, $1.5 \leq k \leq 25000$, $-20 \leq \kappa \leq 20$, $-0.003 \leq \varphi_t \leq 0.28$, $-0.5 \leq \theta_t \leq 0.5$, $0.45 \leq P \leq 1$, $s = 14$.

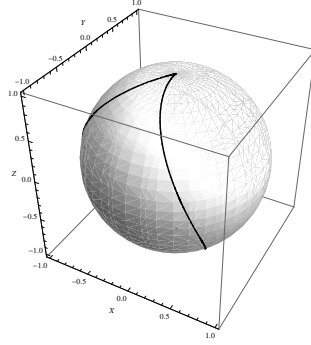


Fig. 5. Apex hodograph at a resonance for initial state $\theta_0 = 0$, $\varphi_0 = \pi/4$; $\omega = H = 0.2$, $h = 0.5$ for a period $T = 2\pi/h$; $0 \leq P \leq 1$, $0.5 \leq v \leq 0.54$, $1 \leq k \leq 1.28$, $-0.64 \leq \kappa \leq 0.64$, $s = 6.53$, $C_{res} = 3.4$.

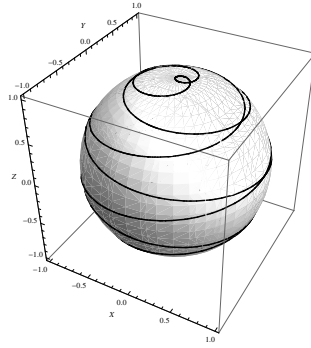


Fig. 6. Hodograph at the resonance for initial state $\theta_0 = 0$, $\varphi_0 = \pi/4$; $\omega = H = 5$, $h = 0.5$, $T = 2\pi/h$; $0 \leq P \leq 1$, $0.47 \leq v \leq 5.02$, $1 \leq k \leq 20$, $-0.55 \leq \kappa \leq 0.55$, $s = 40, 84$, $C_{res} = 160.14$.

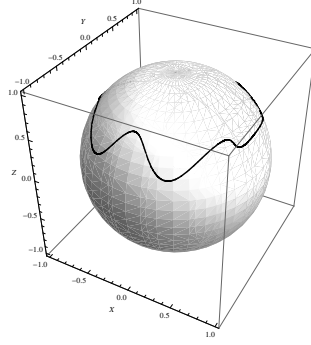


Fig. 7. Apex qubit dynamics in the linearly polarized field with the parameters as in Fig. 3 during 14.66; $0.14 \leq v \leq 0.77$, $1 \leq k \leq 22$, $-200 \leq \kappa \leq 350$, $0.08 \leq \varphi_t \leq 0.87$, $-0.58 \leq \theta_t \leq 0.6$, $0.14 \leq P \leq 0.3$, $s = 6.44$.

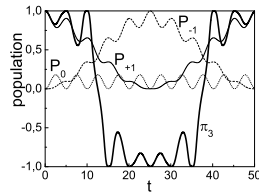


Fig. 8. Populations Eqs. (39) and the third component of the qutrit polarization vector π_3 with the model parameters (for $m = 4$, $n = 5$ in the Eq.(23)) $\omega = H = 0$, $Q = 1$, $h = 3Q/8$ for the full time period $10(2\pi/f)$.

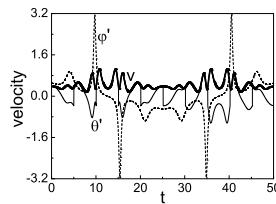


Fig. 9. Time dependence of the velocities of the qutrit apex v , φ' and θ' with the model parameters as in a Fig. 8.

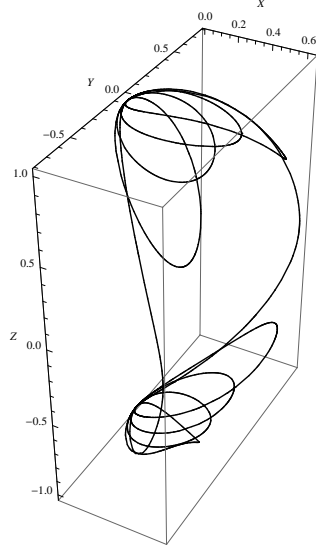


Fig. 10. 3D parametric plot of the qitrit polarization vector $\vec{\pi}(t)$ with the parameters as in Fig. 8. The torsion is small $-10^{-26} < \kappa < 10^{-26}$ and also changes its sign 28 times over the full period, while the curvature varies within $0.005 \leq k \leq 29$; $s = 22.13$.

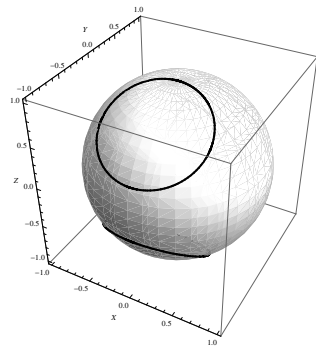


Fig. 11. Hodographs for 2 qitrit polarization vectors on the sphere over the time 25.07; $J = 0.01$, $h_1 = \bar{h}_1 = 0.15$, $h_3 = -\bar{h}_3 = 0.2$; circulations: $C_{up} = 0.53$, $C_{down} = -0.81$.

APPENDIX

The exact solution for the qutrit, taking into account only the anisotropy Q at the start from the northern pole $\rho_{qutrit}(t=0) = \begin{pmatrix} 1 & 0 & 0 \\ 0 & 0 & 0 \\ 0 & 0 & 0 \end{pmatrix}$ in the circularly polarized magnetic field [4] at the resonance $\omega = H$ has the form

$$q_1 = \frac{\sqrt{6}h \sin \frac{ft}{2}}{f^2} \left(f \cos \frac{Qt}{2} \sin \omega t + Q \sin \frac{ft}{2} \cos \omega t \right), \quad (31)$$

$$q_2 = \frac{\sqrt{6}h \sin \frac{ft}{2}}{f^2} \left(Q \sin \frac{ft}{2} \sin \omega t - f \cos \frac{Qt}{2} \cos \omega t \right), \quad (32)$$

$$q_3 = \sqrt{\frac{3}{2}} \left(\frac{Q \sin \frac{ft}{2} \sin \frac{Qt}{2}}{f} + \cos \frac{ft}{2} \cos \frac{Qt}{2} \right), \quad (33)$$

$$q_4 = \frac{1}{f^2} \sqrt{\frac{3}{2}} \left(-2h^2 \sin^2 \frac{ft}{2} \sin 2\omega t + \left(f^2 \cos \frac{ft}{2} \sin \frac{Qt}{2} - fQ \sin \frac{ft}{2} \cos \frac{Qt}{2} \right) \cos 2\omega t \right), \quad (34)$$

$$q_5 = \frac{\sqrt{6}h \sin \frac{ft}{2}}{f} \left(\sin \frac{Qt}{2} \sin \omega t - \cos \frac{ft}{2} \cos \omega t \right), \quad (35)$$

$$q_6 = \frac{h^2 + Q^2 + 3h^2 \cos ft}{\sqrt{2}f^2}, \quad (36)$$

$$q_7 = \frac{\sqrt{6}h \sin \frac{ft}{2}}{f} \left(\cos \frac{ft}{2} \sin \omega t + \sin \frac{Qt}{2} \cos \omega t \right), \quad (37)$$

$$q_8 = \frac{1}{f^2} \sqrt{\frac{3}{2}} \left(f \left(Q \sin \frac{ft}{2} \cos \frac{Qt}{2} - f \cos \frac{ft}{2} \sin \frac{Qt}{2} \right) \sin 2\omega t - 2h^2 \sin^2 \frac{ft}{2} \cos 2\omega t \right), \quad (38)$$

where q_1, q_2, q_3 are the spin components, $f = \sqrt{4h^2 + Q^2}$. The population levels in the qutrit are equal to

$$P_{+1} = \frac{1}{6}(2 + \sqrt{6}q_3 + \sqrt{2}q_6), \quad P_0 = \frac{1}{3}(1 - \sqrt{2}q_6), \quad P_{-1} = \frac{1}{6}(2 - \sqrt{6}q_3 + \sqrt{2}q_6). \quad (39)$$

The qutrit polarization vector is equal to $\vec{\pi}(t) = (q_1, q_2, q_3)/N$, where $N = \sqrt{q_1^2 + q_2^2 + q_3^2}$.

The author wishes to thank I. V. Tanatarov and A. S. Peletminskii for useful comments.

-
- [1] Ivanchenko E.A.: Magnetic resonance in an elliptic magnetic field. *Physica B* **358**, 308 (2005)
- [2] Ivanchenko E.A.: Stabilization magnetic resonance position by synchronized magnetic field. *Low Temp. Phys.* **31**, 577 (2005)
- [3] Abramovitz M., Stegun I.A.: *Handbook of Mathematical Functions* Dover. New York (1968)

- [4] Rabi I.I.: Space quantization in a gyrating field. *Phys. Rev.* **51**, 652 (1937)
- [5] Bambini A., Berman P.R.: Analytic solutions to the two-state problem for a class of coupling potentials. *Phys. Rev. A* **23**, 2496 (1981)
- [6] Bloch F., Siegert A.: Magnetic resonance for nonrotating fields. *Phys. Rev.* **57**(6), 522 (1940)
- [7] Feynman R.P., Vernon J. F. L., Hellwarth R.W.: Geometrical Representation of the Schrödinger Equation for Solving Maser Problems. *J. Appl. Phys.* **28**(1), 49 (1957)
- [8] Goldstein H.: *Classical Mechanics*. Addison-Wesley Publishing Company, INC., Cambridge, Massachusetts (1959)
- [9] Bloch F.: Nuclear Induction. *Phys. Rev.* **70**(7-8), 460 (1946)
- [10] Viola L., Fortunato E.M., Lloyd S., Tseng C.H., Cory D.G.: Stochastic Resonance and Non-linear Response by NMR Spectroscopy. arXiv:/quant-ph/0001095v1 26 Jan (2000)
- [11] Feynman R., Leighton R.B., Sands M.: *The Feynman lectures on physics*. vol. 3 Addison-Wesley Publishing Company, INC., Massachusetts, Palo Alto, London (1965)
- [12] Aminov Y.A.: *Differential geometry and topology of curves*. Nauka, Moscow (1987)
- [13] Ho T.S., Cho S.I.: Semiclassical many-mode Floquet theory III. SU(3) dynamical evolution of three-level systems in intense bichromatic fields. *Phys. Rev. A* **31**(2), 659 (1985)
- [14] Ho T.S., Cho S.I.: Semiclassical many-mode Floquet theory IV. Coherent population trapping and SU(3) dynamical evolution of dissipative three-level systems in intense bichromatic fields. *Phys. Rev. A* **32**(2), 377 (1985)
- [15] Ivanchenko E.A.: Qutrit: entanglement dynamics in the finite qutrit chain in the consistent magnetic field. arXiv:1106.2297v1 [quant-ph] (2011)
- [16] Benenti G., Siccardi S., Strini G.: Non-perturbative interpretation of the Bloch vector's path beyond rotating wave approximation. *Phys. Rev. A* **88**, 033814 (2013)